American Mineralogist, Volume 91, pages 1499–1508, 2006

Identifying the effects of petrologic processes in a closed basaltic system using trace-element concentrations in olivines and glasses: Implications for comparative planetology

JUSTIN J. HAGERTY,[1,3,*] CHARLES K. SHEARER,[1] DAVID T. VANIMAN,[2] AND PAUL V. BURGER[1]

[1]Institute of Meteoritics, Department of Earth and Planetary Sciences, University of New Mexico, MSCO3-2050, Albuquerque, New Mexico 87131-0001, U.S.A.

[2]Los Alamos National Laboratory, Earth and Environmental Sciences, MS D462, Los Alamos, New Mexico 87545, U.S.A.

[3]Current address: Los Alamos National Laboratory, Space Science and Applications, MS D466, Los Alamos, New Mexico 87545, U.S.A.

ABSTRACT

We use trace-element concentrations in olivines and glasses from a closed basaltic system to identify the effects of petrologic processes on the trace-element record of that system. The closed basaltic system in question is the Makaopuhi Lava Lake (MLL), which is closed with respect to magma mixing. Detailed studies of this lava lake have provided important information about system variables and petrologic processes that have been measured and observed at the lake. These previous studies show that olivine crystallized from the lava lake at all stages of the lake's evolution, which means that olivine and residual glasses contain a record of the lake's petrologic history. We use this information, in conjunction with variations in trace-element concentrations in olivines and glasses, to show that mineral crystallization, gravitational settling, convective flow, filter pressing, and mineral-melt interface kinetics have characteristic effects on the trace element record of a closed basaltic system. These results are pertinent to the field of comparative planetology because they can be used to evaluate petrologic information in small samples from other planetary bodies, where information about system variables and/or petrologic processes is limited.

Keywords: Makaopuhi Lava Lake, Hawaii, Basalt, Trace Elements and REE, Distribution Coefficients, Olivine, Glass, Comparative Planetology, Geochemistry

INTRODUCTION

The field of comparative planetology has used knowledge from well-studied geologic systems on the earth, in conjunction with analyses of small extraterrestrial samples, to make implications for planetary environments where we have little information about system variables and petrologic processes. For example, some workers have used microbeam analyses of individual minerals in terrestrial and extraterrestrial samples to compare basaltic systems on different planetary bodies (e.g., Papike 1981, 1996, 1998; Papike et al. 1998, 2003). More specifically, these workers have used the compositions and atomic structures of individual minerals to obtain information about the physical and chemical conditions under which basaltic systems formed and evolved.

We propose that another tool can be added to this petrologic skill set by using variations in the concentrations of trace elements in olivines and glasses to identify the effects of petrologic processes in basaltic systems. This can be accomplished by using detailed observations and measurements from a closed basaltic system (i.e., Makaopuhi Lava Lake, Hawaii) to test the impact of complexing factors on partitioning behavior of trace elements between olivines and melts. We show that deviations from the expected partitioning behavior of trace elements between olivines and melts (i.e., glasses) can be used to identify the effects of gravitational settling, convective transport, filter pressing, mineral-melt interface kinetics, and unintentional analysis of submicroscopic melt inclusions. These findings, in turn, can be used to interpret the results of microbeam analyses of extraterrestrial samples, such that the effects of both large-scale and small-scale processes can be identified in basaltic systems on other planetary bodies.

MAKAOPUHI LAVA LAKE

Hawaiian lava lakes are unique natural laboratories that illustrate the physical and chemical evolution of closed basaltic systems. One of the best-studied lakes is the Makaopuhi Lava Lake (MLL), which was formed during the 1965 eruption of the Kilauea volcano (Wright and Okamura 1977). This 365 m diameter, 83 m deep, lava lake was studied in great detail by the United States Geological Survey (USGS) between March 1965 and February 1969. During that time, the USGS took direct measurements of the lava lake's temperature, oxygen fugacity, volatile content, petrography-chemistry, viscosity, and density (Wright and Okamura 1977). Information derived from these observations shows that gravitational settling, convective flow, and the formation of liquid segregations via filter pressing, played significant roles in the evolution of the MLL (Wright and Okamura 1977). These detailed physical and chemical measurements from the MLL, provide a natural laboratory for

* E-mail: jhagerty@lanl.gov

observing the chemical and physical changes that occur in an evolving basaltic magma. We use this information, along with microbeam analyses of silicate phases (e.g., Papike 1981, 1996, 1998; Papike et al. 1998, 2003), to make a correlation between well-documented petrologic processes and information retained in the trace-element record of olivines and glasses. We use olivines and glasses for this task because these phases retain a record of the MLL's entire petrologic history (Wright and Okamura 1977). We use trace-element concentrations in this study because they are very sensitive to the processes of magmatic differentiation (Hess 1989).

Analytical approach

All of the samples analyzed in this study were selected based on their collection temperatures and glass abundance. All analyzed samples contain at least 18% glass, thus making it possible to determine the olivine-melt distributions of major, minor, and trace elements. Samples M-18, M23-24, M21-26, M22-18, M1-6, and M5-13 were collected at temperatures between 1160 and 1050 °C (see Table 1) and at an oxygen fugacity between the FMQ and Ni-NiO buffers (see Fig. 1).

The concentrations of selected major, minor, and trace elements were measured in both glass and olivine. All samples were imaged and mapped for textural and mineralogical characteristics using a JEOL 5800LV scanning electron microscope (SEM) with an attached Oxford Isis Series 300 energy dispersive microanalytical system. The SEM was optimized for high-resolution imaging, which requires a 20 kV acceleration voltage, a sample current of 20 nA, a spot size of 8–10 µm, and a working distance of 8–16 mm.

The major- and minor-element concentrations were obtained by using a JEOL JXA-8200 electron probe microanalyzer at the University of New Mexico. This instrument is equipped with a back-scattered electron detector, a thin-window energy dispersive spectrometer (EDS), and five wavelength dispersive spectrometers (WDS). The following analytical conditions were used during this study: 15 kV accelerating voltage, a 20 nA beam current, a 1 µm spot size for analyses of minerals, and a 10 µm spot size for analyses of glass. The larger spot size for the glass analyses reduces loss of volatile and moderately volatile species such as K_2O, P_2O_5, Na_2O, and H_2O.

Trace-element concentrations in the Makaopuhi samples were measured using a Cameca ims 4f secondary ion mass spectrometer (SIMS) located at the University of New Mexico. The primary ion beam consisted of mass-filtered $^{16}O^-$ ions, which were accelerated through a nominal potential of 10 kV. Sputtered secondary ions were energy filtered using a sample-offset voltage of –75 V as well as an energy window of ±25 V. A beam current of 15 nA and a beam size of ~15 µm were used to measure ^{39}K, ^{51}V, ^{52}Cr, ^{55}Mn, ^{59}Co, ^{60}Ni, ^{89}Y, ^{147}Sm, and ^{232}Th in olivine and glass. During these measurements, background peak positions were counted to monitor detection noise. Absolute concentrations of each element were calculated using empirical relationships of trace element/$^{30}Si^+$ ratios, which in turn were normalized to SiO_2 content derived from electron microprobe analyses. The trace-element concentrations of the glass and olivine standards span a large range of compositions and bracket the range of compositions expected in the unknowns. All analytical errors are reported as 1-sigma standard deviations (STD).

Table 1. Sample description (see Wright and Okamura 1977 for details)

	M-18	M23-24	M21-26	M22-18	M1-6	M5-13
Collection Temp (°C)	1160*	1145†	1130*	1110*	1070‡	1050‡
Collection depth (ft)	surface	24	26	21	7	11
Glass (modal %)	86	80	75	72	40	18
Olivine (modal %)	5.5	2	3	2	1.5	1.6
Augite (modal %)	6.2	8	12	14	36	45
Plagioclase (modal %)	0.4	7	10	12	20	29
Ilmenite (modal %)	–	–	–	–	1	6
Others (modal %)	1.9	3	–	–	1.5	0.4

* Reported by Wright and Okamura (1977).
† Calculated by Wright and Okamura (1977), assuming >78% glass in the sample.
‡ Reported by Hakli and Wright (1966).

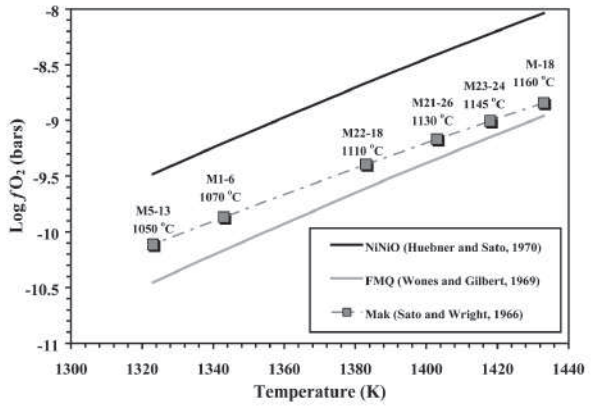

Figure 1. Log f_{O_2} vs. temperature diagram showing the calculated oxygen fugacities for samples from the Makaopuhi Lava Lake. The equation of Sato and Wright (1966) was used to calculate f_{O_2}.

Results

Major and minor elements

Glass. Major-element concentrations in glasses from the Makaopuhi Lava Lake show a variety of changes as a function of temperature (Table 2; Figs. 2a and 2b). The concentrations of K_2O, Na_2O, P_2O_5, and FeO in the glass increase with decreasing temperature (Figs. 2a and 2b). Conversely, the concentrations of Al_2O_3, CaO, and MgO all decrease with decreasing temperature (Figs. 2a). The concentration of TiO_2 increases in the glass with decreasing temperature through 1070 °C and then decreases due to the crystallization of ilmenite (Fig. 2a).

Olivine. All of the olivines analyzed in this study show limited variations in the concentrations of major elements (i.e., limited zoning) and hence they exhibit a relatively restricted range in forsterite content (Fo_{81} to Fo_{78}). However, Wright and Okamura (1977) showed that olivine compositions range from Fo_{85} to Fo_{50}. The wide compositional range measured by Wright and Okamura (1977) could be a function of analyzing partially resorbed olivines in relatively low-temperature samples, which we avoided intentionally. The olivines analyzed in this study show little or no variation in CaO (0.26–0.33 ± 0.04 wt%), MnO (0.24–0.28 ± 0.03 wt%), TiO_2 (0.01–0.08 ± 0.01 wt%), and Cr_2O_3 (0.01–0.03 ± 0.01 wt%). The olivine grains show no significant changes in the major-element concentrations with decreasing temperature or with changes in depth.

Trace elements

Glass. Glass analyses were collected adjacent to the olivine phenocrysts (i.e., within 15–50 µm) and along traverses away from growth surfaces of the phenocrysts (Fig. 3) to determine if there is a compositional gradient between the olivines and the adjacent melts. The ion-microprobe results from this study show that the glasses adjacent to olivine grains in sample M-18 (i.e., the highest temperature sample) have surprisingly high concentrations of incompatible trace elements compared to the glasses in other Makaopuhi samples and to other regions of glass within M-18 (Tables 3 and 4; Figs. 4a and 4b). In other words, the data show that the trace-element concentrations in the glasses vary as a function of distance from the olivine phenocrysts. Regions

of glass far from olivine phenocrysts (i.e., "normal glass" in Table 4) are compositionally similar to one another, whereas glasses within 15–50 μm (i.e., "Ol-glass" in Table 4) show a compositional gradient. The magnitude of the compositional difference between glasses far from phenocrysts and those near phenocrysts decreases with decreasing temperature. Wright and Okamura (1977) indicated that sample M-18, which was collected at the time of the eruption, represents the initial melt composition, which means that the glasses in sample M-18 provide compositional baselines against which lower-temperature glass compositions can be compared.

Glasses in low-temperature samples from MLL show a substantial increase in the concentrations of incompatible elements such as Y, Ce, Sm, Eu, Yb, and Th (Table 3; Figs. 4a and 4b), compared to high-temperature samples. Yttrium, Ce, Sm, Eu, Yb, and Th are deemed incompatible because they do not easily fit into the crystal structures of the crystallizing mineral assemblage and are therefore concentrated in the residual magma. However, the concentrations of V, Mn, Ni, and Co, as expected, are affected by the crystallization of specific minerals. For example, below 1070 °C, V, Mn, Ni, and Co show a sharp decrease in their concentrations (Figs. 4a and 4b). The decreasing concentrations of these elements are coincident with the crystallization of ilmenite. The significant decrease in the concentration of Cr with decreasing temperature (Fig. 4a) may be also interpreted as being caused by the simultaneous crystallization of at least three minerals that preferentially incorporate Cr into their structures (i.e., pyroxene, chromite, and ilmenite).

Previous studies of Ni and Co behavior in basaltic systems show that the concentrations of Ni, and to a lesser extent Co, should decrease in the melt as a function of olivine crystallization (Papike et al. 1999). The behavior of Ni in olivine during the petrogenesis of basalts has been well documented by Hart and Davis (1978), Kinzler et al. (1990), and Papike et al. (1999). The distribution of Ni between olivine and melt is dependent on composition (i.e., MgO content) but shows little or no dependence on temperature or pressure (Hart and Davis 1978). Figure 4a indicates that the glasses from the MLL show a decrease in the concentration of Ni with decreasing temperature but a slight increase, followed by a decrease, in the concentration of Co with decreasing temperature.

Olivine. Small, unzoned olivine grains from sample M-18 show unusual trace-element concentrations with respect to olivine grains in the other Makaopuhi samples (Table 5; Fig. 5). For example, the concentrations of incompatible elements such as Y, Sm, and Th are anomalously high in M-18, whereas the concentrations of compatible elements such as Ni, Co, and Mn are lower than expected (Table 5; Fig. 5). If the olivine grains in M-18 were among the first olivines to crystallize from the lake, they should be relatively enriched in compatible elements compared to olivine grains in other MLL samples. The anomalous concentrations described above can be seen in

TABLE 2. Major element concentrations in basaltic glass (wt%)

Sample	SiO_2	TiO_2	Al_2O_3	FeO	MgO	CaO	Na_2O	K_2O	P_2O_5	Total	X_{Mg}	(N)
M-18 (1160 °C)	**50.3**	**2.7**	**13.6**	**11.5**	**5.9**	**11.0**	**2.3**	**0.53**	**0.17**	**98.0**	**48**	**15**
1-sigma STD	0.36	0.17	0.47	0.66	0.75	0.33	0.19	0.08	0.02	0.57		
M23-24 (1145 °C)	**50.8**	**3.2**	**13.4**	**11.7**	**5.7**	**10.3**	**2.4**	**0.65**	**0.17**	**98.3**	**47**	**15**
1-sigma STD	0.55	0.12	0.19	0.60	0.31	0.15	0.13	0.04	0.03	0.74		
M21-26 (1130 °C)	**50.6**	**3.5**	**13.7**	**11.4**	**5.8**	**10.0**	**2.6**	**0.69**	**0.15**	**98.5**	**46**	**12**
1-sigma STD	0.11	0.04	0.22	0.36	0.31	0.12	0.07	0.03	0.00	0.26		
M22-18 (1110 °C)	**50.5**	**3.7**	**13.3**	**12.0**	**5.3**	**9.5**	**2.7**	**0.81**	**0.17**	**98.0**	**44**	**27**
1-sigma STD	0.23	0.04	0.11	0.32	0.17	0.08	0.04	0.03	0.01	0.41		
M1-6 (1070 °C)	**50.5**	**5.1**	**12.1**	**13.8**	**5.1**	**8.4**	**2.9**	**1.09**	**0.23**	**99.2**	**35**	**15**
1-sigma STD	0.40	0.10	0.19	0.57	0.14	0.09	0.15	0.05	0.03	0.76		
M5-13 (1050 °C)	**50.9**	**3.0**	**11.3**	**14.9**	**4.2**	**7.6**	**3.6**	**1.92**	**0.54**	**98.0**	**35**	**15**
1-sigma STD	0.52	0.30	0.77	0.60	0.54	0.34	0.53	0.08	0.06	0.67		

Note: (N) = number of analyses. X_{Mg} = mol%[MgO/(MgO + FeO)] × 100.

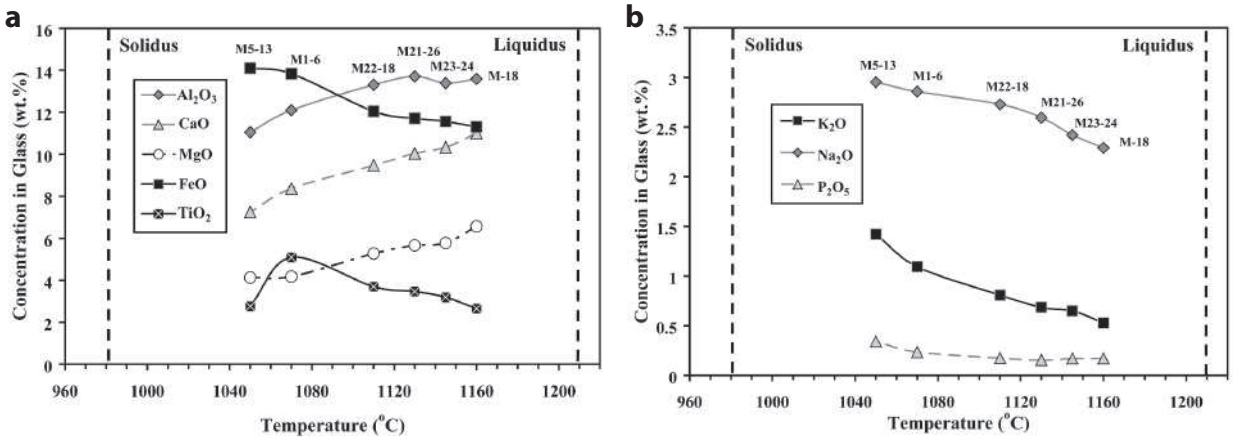

FIGURE 2. Major element composition of the basaltic glass plotted as a function of decreasing temperature. (**a**) Note the decrease in the concentration of TiO_2 after ilmenite comes onto the liquidus (i.e., after 1070 °C). (**b**) K_2O and Na_2O concentrations increase in the glass with increasing crystallization.

TABLE 3. Trace element concentrations in basaltic glass (ppm)

Sample	K	V	Cr	Mn	Co	Ni	Y	Ce	Sm	Eu	Yb	Th	Th/Sm	(N)
M-18 (1160 °C)	**4827**	**320**	**264**	**1451**	**59.2**	**232**	**29.3**	**39.8**	**6.4**	**2.4**	**2.3**	**1.8**	**0.28**	**5**
1-sigma STD	52.9	4.7	7.1	38.5	5.8	20.3	1.6	1.0	0.64	0.02	0.02	0.2	0.03	
M-18 (1160 °C)#	**4660**	**339**	**265**	**1435**	**69.5**	**243**	**22.5**	**38.7**	**6.3**	**2.4**	**2.8**	**1.2**	**0.28**	**4**
1-sigma STD	134	8.6	3.4	3.4	1.1	3.0	0.55	1.7	0.09	0.07	0.20	0.02	0.01	
M23-24 (1145 °C)	**5634**	**320**	**116**	**1524**	**65.2**	**223**	**36.4**	**50.7**	**7.8**	**3.0**	**3.1**	**1.9**	**0.24**	**5**
1-sigma STD	20.3	9.2	9.3	52.5	0.9	8.0	2.8	0.61	0.47	0.04	0.01	0.10	0.02	
M21-26 (1130 °C)	**5516**	**336**	**107**	**1647**	**60.7**	**216**	**35.1**	**53.3**	**8.5**	**3.1**	**3.0**	**2.0**	**0.24**	**5**
1-sigma STD	76.7	3.5	4.6	28.6	4.4	2.7	2.9	0.79	0.60	0.08	0.20	0.22	0.02	
M22-18 (1110 °C)	**6432**	**337**	**58**	**1754**	**65.6**	**208**	**35.3**	**57.1**	**9.0**	**3.7**	**3.6**	**2.2**	**0.23**	**5**
1-sigma STD	89.2	7.1	2.5	23.2	2.1	1.8	2.3	1.9	0.75	0.07	0.02	0.36	0.03	
M1-6 (1070 °C)	**8750**	**392**	**16**	**2063**	**74.3**	**205**	**48.5**	**72.2**	**10.5**	**4.1**	**4.0**	**2.4**	**0.23**	**5**
1-sigma STD	183	7.2	1.1	18.5	1.1	5.3	1.7	3.6	0.55	0.08	0.25	0.29	0.02	
M5-13 (1050 °C)	**12011**	**244**	**10**	**1794**	**58.9**	**165**	**66.9**	**99.1**	**12.0**	**5.5**	**5.2**	**2.9**	**0.24**	**5**
1-sigma STD	788	6.5	0.37	50.3	1.1	2.6	2.3	2.0	0.62	0.19	0.45	0.11	0.01	

Notes: (N) = number of analyses; # = Glass analyses conducted >15 micrometers away from phenocrysts.

TABLE 4. Glass compositions in sample M-18 (ppm)

Sample	V	Cr	Mn	Co	Ni	Y	Sm	Th
M-18 Ol-glass	343	253	1430	49.6	191	35.6	7.3	2.4
M-18 Ol-glass	347	251	1410	44.5	191	35.6	6.9	2.7
M-18 Ol-glass	342	252	1390	41.1	191	35.8	7.8	2.4
M-18 Ol-glass	345	254	1399	48.2	191	35.6	7.4	2.5
M-18 Ol-glass	346	254	1435	47.4	190	36.5	7.6	2.2
Average	345	253	1413	46.2	191	35.8	7.4	2.4
M-18 Normal glass	341	262	1433	69.0	240	22.8	6.3	1.2
M-18 Normal glass	338	262	1439	68.6	245	22.2	6.1	1.2
M-18 Normal glass	336	268	1437	69.5	244	22.9	6.3	1.2
Average	338	264	1437	69.0	243	22.6	6.2	1.2

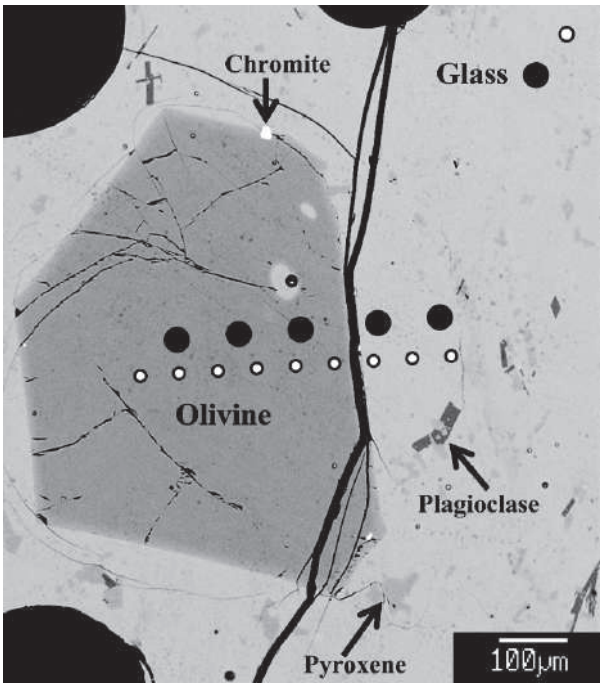

FIGURE 3. Back-scattered electron image of a large olivine grain in sample M21-26. The consecutive dots in this image represent microbeam traverses from olivine into glass. The large black dots represent SIMS points and the small white dots represent electron microprobe points. Analytical points in the glasses were conducted separately from the olivine analytical points due to differences in the analytical conditions. The two points in the upper right portion of the image represent SIMS and electron microprobe points that were taken to determine the glass composition far away from any phenocrysts.

Figure 6, which shows the unusual Y and Ni concentrations in sample M-18 relative to the other samples. Figure 6 also shows that the range of trace-element compositions in the olivines becomes larger with decreasing temperature (e.g., the range of Ni concentrations in sample M23-24 is smaller than the range seen in sample M1-6).

Olivine grains in sample M23-24 are small, unzoned, and exhibit high concentrations of compatible elements such as Ni and Co, as well as low concentrations of incompatible elements such as Y and Th (Fig. 5). Thin sections from M21-26, M22-18, M1-6, and M5-13 have large olivine crystals that appear to be zoned with respect to trace-element concentrations. These large olivine phenocrysts have K, V, Y, Sm, and Th concentrations that increase from core to rim, whereas the concentrations of Mn, Co, and Ni decrease from core to rim (Table 5). Inspection of Table 5 shows that Cr concentrations in the large olivine grains decrease from core to rim but that the absolute concentrations of Cr also increase with decreasing temperature. The increase in Cr concentration with decreasing temperature appears to be related to the abundance of chromite inclusions within the analyzed olivine grains, which increases curiously from high-temperature to low-temperature samples (e.g., Wright and Okamura 1977).

DISCUSSION

Three large-scale differentiation processes were observed during the USGS study of the Makaopuhi Lava Lake, including gravitational settling, convective flow, and formation of liquid segregations via filter pressing (Wright and Okamura 1977). We use information about these geologic processes and the associated system variables (e.g., Wright and Okamura 1977), along with variations in the concentrations of major, minor, and trace elements, to determine how gravitational settling, convective flow, liquid segregations, mineral crystallization, and mineral-

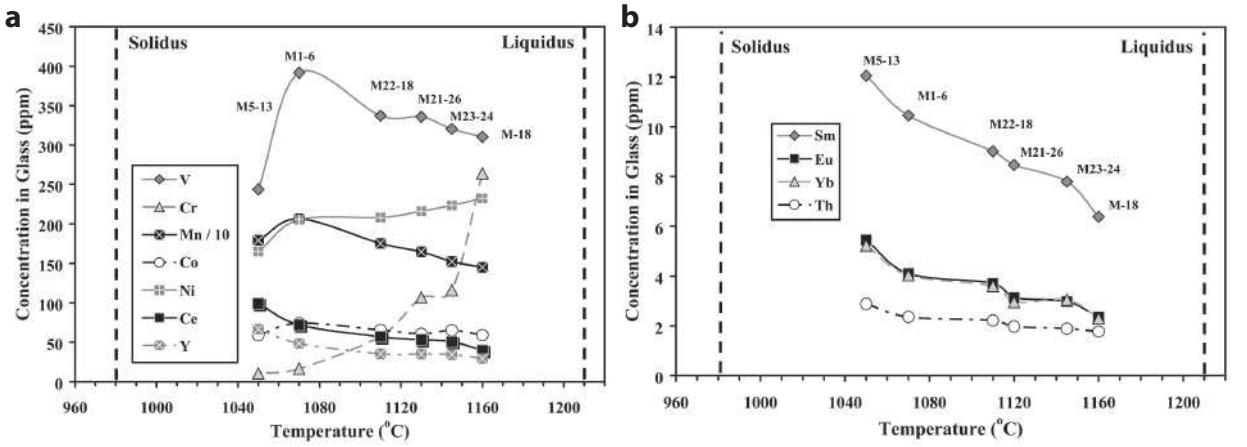

FIGURE 4. Trace-element composition of the basaltic glass plotted as a function of temperature. (**a**) Note the unusual concentrations of samples M-18 and M5-13. (**b**) The concentration of each element increases with decreasing temperature, thus reflecting the incompatible nature of the elements with respect to olivine, pyroxene, plagioclase, and ilmenite.

melt interface kinetics can affect the trace element record of a closed, basaltic system.

MECHANISMS AFFECTING THE DISTRIBUTION OF MAJOR, MINOR, AND TRACE ELEMENTS

Mineral crystallization and filter pressing. The basaltic glasses in the Makaopuhi samples have major-, minor-, and trace-element concentrations that vary as a function of mineral crystallization. The effects of mineral crystallization can be seen in a direct comparison of Figure 7 with Figures 2a, 2b, 4a, and 4b. A comparison of Figures 7 and 2a shows that the continuous decrease in the concentrations of both Al_2O_3 and CaO in the glass corresponds to and reflects the gradual increase in plagioclase abundance with increasing crystallization. A comparison of Figures 7 and 4a shows that the decrease in Cr concentration in the glass coincides with the increasing crystallization of chromite, augite, and ilmenite (Fig. 7), all of which preferentially incorporate Cr into their mineral structures (Ringwood 1970; Hart and Dunn 1993). A comparison of Figures 7, 2a, and 4a shows that the concentrations of TiO_2, V, Mn, Co, and Ni increase in the glass with decreasing temperature until ilmenite begins to crystallize at approximately 1070 °C. As expected, these examples show various ways in which mineral crystallization can affect the trace-element record of the evolving basaltic melt. We can use these expected behaviors and processes to help identify other petrologic mechanisms in the MLL.

For example, we assume that the amount of crystallization that a given sample has experienced should be directly proportional to the percentage of glass remaining in that sample. In other words, if a given sample has seen 70% crystallization, we would expect to see approximately 30% glass remaining in that sample. Given this information, it should be possible to calculate the amount of crystallization that a given sample has experienced. The degree of crystallization can be determined by solving the basic crystallization equation $[C_l/C_o = F^{(\bar{D}-1)}]$ for F. Here, C_l = concentration of element in the melt, C_o = concentration of element in the parent, $\bar{D}$ = bulk partition coefficient, and F = fraction of melt remaining. This crystallization equation can

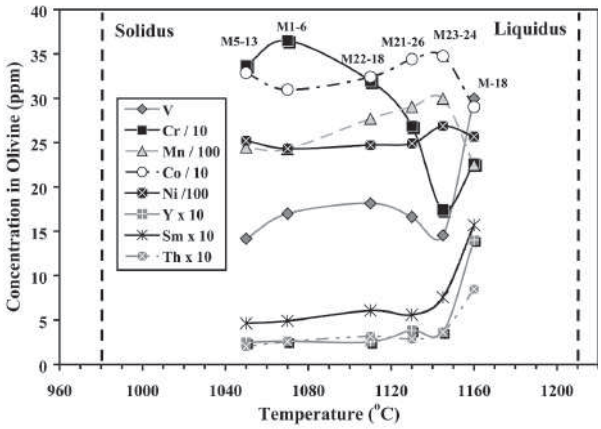

FIGURE 5. Trace-element concentrations in olivine plotted as a function of temperature. The concentrations of several elements were adjusted so that all elements could be plotted on the same diagram. Note the concentration variations in the high- and low-temperature samples. The unusual pattern for Cr may be affected by chromite inclusions.

be simplified to $C_l/C_o = F$ by eliminating the bulk partition coefficient. The bulk $\bar{D}$-value can be eliminated if the elements of interest are incompatible in the crystallizing mineral assemblage (i.e., the bulk $\bar{D}$-value is zero). Fortunately, Y and Ce are both highly incompatible in olivine, plagioclase, pyroxene, chromite, and ilmenite, which means that the bulk $\bar{D}$-values for Y and Ce are essentially zero for the crystallizing mineral assemblage. The variable, C_o, represents the concentration of Y and Ce in basaltic glass in sample M-18 (i.e., the initial melt composition or parent); whereas C_l represents the concentrations of Y and Ce in the other Makaopuhi samples (i.e., the residual melts). Dividing C_l by C_o produces values of F that are plotted in Figure 8.

Figure 8 compares the calculated F value (percent melt calculated) to the percentage of glass that is present in a given sample (see Table 1 for glass abundance). If crystallization is the dominant mechanism in the Makaopuhi Lava Lake, the calculated melt (F) should plot on a 1:1 line with the modal abundance of

TABLE 5. Trace element concentrations in olivine (ppm)

Sample	K	V	Cr	Mn	Co	Ni	Y	Sm	Th	(N)
M-18 (1160 °C)	**83.1**	**30.0**	**226**	**2251**	**290**	**2566**	**1.4**	**1.6**	**0.85**	**6**
1-sigma STD	9.7	5.5	16.3	135	19.4	87.2	0.64	0.11	0.04	
M23-24 (1145 °C)	**6.0**	**14.6**	**174**	**2994**	**347**	**2686**	**0.36**	**0.76**	**0.36**	**6**
1-sigma STD	0.76	0.81	11.8	119	7.8	55.20	0.02	0.03	0.04	
M21-26 (1130 °C)	**5.8**	**16.6**	**268**	**2902**	**344**	**2677**	**0.38**	**0.56**	**0.29**	**8**
1-sigma STD	1.04	1.73	21.9	143	12.6	112	0.02	0.02	0.03	
Core avg.	2.6	16.0	281	2942	347	2760	0.29	0.55	0.29	
Rim avg.	4.9	17.3	256	2848	340	2594	0.33	0.57	0.28	
M22-18 (1110 °C)	**4.7**	**18.1**	**319**	**2769**	**324**	**2471**	**0.25**	**0.61**	**0.32**	**7**
1-sigma STD	0.57	0.68	30.7	58.3	8.6	115	0.02	0.05	0.02	
Core avg.	4.6	18.1	328	2788	326	2560	0.25	0.60	0.32	
Rim avg.	4.9	18.2	313	2749	321	2404	0.26	0.62	0.32	
M1-6 (1070 °C)	**24**	**17.0**	**365**	**2428**	**310**	**2432**	**0.26**	**0.49**	**0.26**	**9**
1-sigma STD	3.96	1.01	37.0	212	25.8	104	0.03	0.07	0.03	
Core avg.	25	16.8	383	2606	324	2489	0.26	0.49	0.24	
Rim avg.	28	17.2	342	2285	298	2360	0.26	0.54	0.26	
M5-13 (1050 °C)	**9.6**	**14.2**	**374**	**2444**	**329**	**2521**	**0.25**	**0.46**	**0.20**	**8**
1-sigma STD	1.91	1.5	42	408	18	102	0.01	0.06	0.01	
Core avg.	7.87	12.6	384	2537	335	2603	0.23	0.43	0.19	
Rim avg.	11.35	15.7	365	2338	320	2438	0.27	0.50	0.21	

Note: (N) = number of analyses.

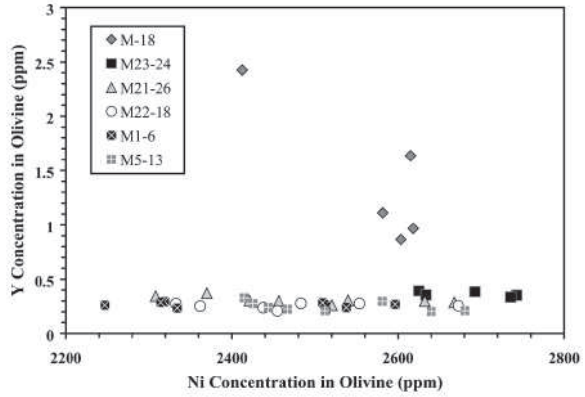

FIGURE 6. Concentrations of Y and Ni in olivine. The data for sample M-18 are affected by melt inclusions that have trace-element concentrations similar to the bulk melt. Note the wide range in the Ni concentrations for sample M5-13.

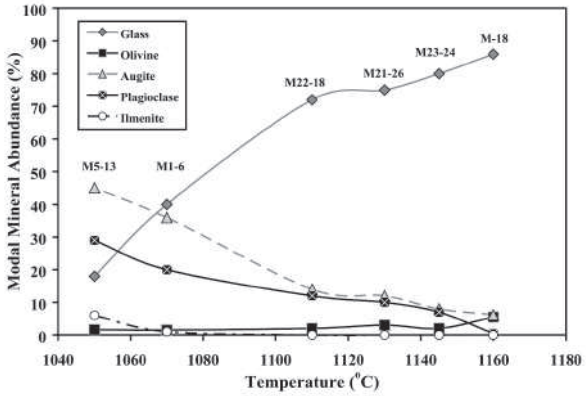

FIGURE 7. Variation of the modal abundances as a function of temperature. Note that ilmenite increases in abundance from 1 to 6% between 1070 and 1050 °C. The drastic increase in ilmenite crystallization significantly depletes the concentrations of several elements in glasses at 1070 and 1050 °C.

glass (Fig. 8). Figure 8 shows that the percentages of melt and glass agree quite well in the high-temperature sample (1145 °C). However, as the temperature decreases, the Makaopuhi samples deviate significantly from the idealized line (Fig. 8), indicating that the amount of glass observed in the samples is less than what was calculated using the crystallization equation. One way to reduce the amount of melt in any given sample is through filter pressing, a mechanism that led to the production of segregation veins at the MLL (e.g., Wright and Okamura 1977). Filter pressing occurs when a given mass compresses a mixture of minerals and melt, forcing the melt toward regions of lower pressure (Hess 1989). The mineral assemblage that is left behind will have a relatively low modal abundance of glass, similar to what we see in samples from the MLL.

Gravitational settling and convective transport. Previous studies of MLL have shown that gravitational settling and convective transport of olivine played an important role in the evolution of the lava lake (e.g., Wright and Okamura 1977). Wright and Okamura (1977) showed that large olivine phenocrysts (i.e., >1 mm) became concentrated near the bottom of the lake, while smaller olivine grains may have been transported, along with augite and plagioclase, to other portions of the lake via convective flow. If these processes did indeed play major roles in the evolution of the lava lake, many of the olivines would have been separated from their parental liquids and would therefore be out of equilibrium with the melts/glasses that they currently are located next to.

Previous workers have shown that if olivine phenocrysts are in equilibrium with the adjacent melt, the calculated Fe-Mg exchange coefficient (K_D) between olivine and the adjacent melt should equal 0.30 ± 0.03 (i.e., Roeder and Emslie 1970). However, the exchange K_D for the highest temperature sample (M-18) is much lower (0.21) than the equilibrium value of 0.30 ± 0.03 (see Table 6), thus indicating that the olivines in M-18 were not in equilibrium with the adjacent melt. The observed disequilibrium could be a result of olivine grains forming in the magma prior to eruption into the lava lake (e.g., McBirney 1984). This assertion is supported by the presence of partially

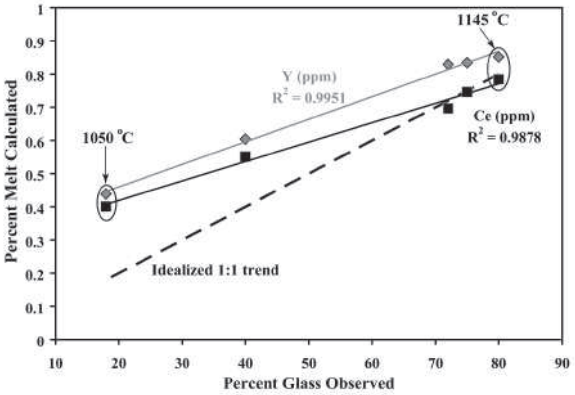

FIGURE 8. Comparison of calculated melt remaining vs. the amount of glass that currently exists within the Makaopuhi thin sections. The percentage of melt remaining was calculated by dividing the trace-element concentration in the glass of sample M-18 by the trace-element concentrations in the glasses of the other Makaopuhi samples. Ideally, the percent melt remaining should be equal to the percentage of glass in the sample. Deviation from the 1:1 line can provide petrogenetic information (see text for discussion).

resorbed phenocrysts in some of the high-temperature samples (e.g., Fig. 9).

Sample M23-24 has a K_D of approximately 0.27, which is within the ±0.03 range of equilibrium described by Roeder and Emslie (1970) (Table 6). However, the other samples have exchange K_D values that become progressively lower with decreasing temperature (Table 6). Table 6 shows that the two lowest temperature samples (M1-6 and M5-13) are farthest from the equilibrium values, thus suggesting that early crystallizing olivine settled under the influence of gravity into melt that was not in equilibrium with the olivine. This observation is reflected in the Ni and Co abundances in the melt (Fig. 4a; Table 3), which do not decrease in the melt as would be expected if olivine had crystallized from the adjacent melt (e.g., Papike et al. 1999). Figure 6 also shows that lower-temperature samples from the MLL have a larger range of Ni concentrations in olivine than do the higher-temperature samples. The increase in the range of Ni concentrations in the olivines with decreasing temperature indicates that the olivine grains formed from different melts with different Ni concentrations.

Figure 4a shows that the Cr concentration in the glasses decreases with the increasing crystallization and Table 5 shows that the absolute concentration of Cr in olivine increases with decreasing temperature. In other words, Cr-rich olivines in low temperature samples are directly adjacent to relatively Cr-poor glasses. Because olivine does not incorporate Cr as efficiently as pyroxene, ilmenite, and spinel, it is assumed that the Cr depletion in the adjacent glasses is not a result of olivine crystallization. These olivines must have formed from relatively Cr-rich melts, which our data indicate were present at the early stages of crystallization (see Fig. 4a). This information, in conjunction with the exchange K_D values and Ni and Co concentration data in the low-temperature samples, indicates that these olivines are out of equilibrium with the adjacent melts and must have been transported to different portions of the lake via gravitational settling and/or convective flow.

TABLE 6. Fe-Mg data for olivine and glass

Sample	MgO wt% (Olivine)	FeO wt% (Olivine)	MgO wt% (Glass)	FeO wt% (Glass)	K_D
M-18 (1160 °C)	41.5	17.0	5.9	11.5	0.21
M23-24 (1145 °C)	38.9	21.2	5.7	11.7	0.27
M21-26 (1130 °C)	40.4	19.9	5.8	11.4	0.25
M22-18 (1110 °C)	40.1	21.3	5.3	12.0	0.23
M1-6 (1070 °C)	40.3	19.3	5.1	13.8	0.18
M5-13 (1050 °C)	40.6	20.1	4.2	14.9	0.14

Mineral-melt interface kinetics. The trace-element data from this study show that there are compositional gradients between olivine phenocrysts and adjacent glasses in sample M-18 (e.g., Table 4). These compositional gradients could be the result of mineral-melt interface processes such as disequilibrium-induced diffusion (e.g., Chakraborty 1995). Recall that some of the olivine phenocrysts in the MLL sample are partially resorbed (Fig. 9), which indicates that the olivines were not in equilibrium with the surrounding melt (e.g., McBirney 1984). The lack of equilibrium between the olivines and the surrounding melt most likely led to diffusion (e.g., Kirkpatrick 1977; Chakraborty 1995; Bindeman and Davis 1999). As diffusion began, incompatible trace elements were mobilized preferentially (e.g., Bindeman and Davis 1999), thus creating a boundary layer between the olivine and the melt. The resulting boundary layer would have high concentrations of incompatible trace elements but low concentrations of compatible trace elements, similar to what we see in sample M-18. The interplay between crystal-growth rate, trace-element diffusion, and interface attachment has been shown to control the composition of the growing phenocryst and the residual melt (e.g., Grove and Raudsepp 1978). Knowledge of these kinetic controls makes it possible to determine if large or small-scale mechanisms are responsible for variations in the trace-element record. In other words, if mineral-melt interface reactions are responsible for variations in the trace-element record of a given sample, the glass analyses will have anomalously high concentrations of incompatible elements and anomalously low concentrations of compatible elements.

Apparent distribution coefficients

As we have shown above, a suite of related samples from a basaltic system can be used to obtain a wealth of information about the petrogenesis of that system. However, in many instances, samples from other planetary bodies are small and compositionally unique, thus making it difficult to relate samples to one another, let alone obtain petrogenetic information from those samples. However, if a given sample contains abundant glass (i.e., >18 modal%) it will be possible to calculate mineral-melt distribution coefficients, which can provide information about the petrogenesis of a given sample. This is because mineral-melt distribution coefficients for trace elements (*D*-values) can be used to test and evaluate models of igneous processes (Grove and Bence 1979). The traditional method for calculating *D*-values involves dividing the concentration of element *x* in a given mineral by the concentration of the same element in the adjacent glass. However, as we have noted above, there are several complicating factors that must be considered when calculating *D*-values. For instance, diffusion, interface-attach-

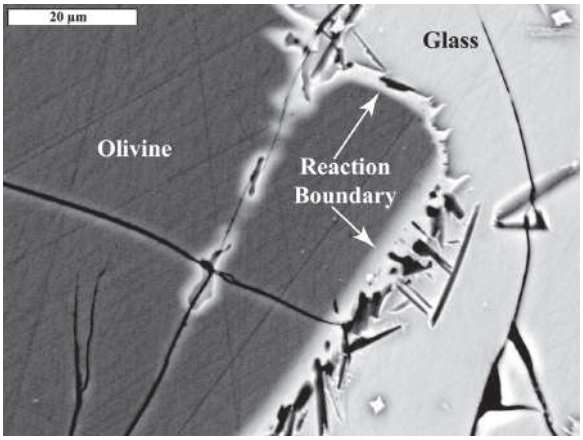

FIGURE 9. Back-scattered electron image of a partially resorbed olivine phenocryst from the Makaopuhi Lava Lake. The reaction boundary represents the disequilibrium between the olivine and the glass.

TABLE 7. Calculated *D*-values derived from concentrations in olivines and their adjacent melts

Sample	V	Cr	Mn	Co	Ni	Y	Sm	Th
M-18 (1160 °C)	0.09	0.86	1.5	4.6	11.7	0.05	0.20	0.30
M23-24 (1145 °C)	0.06	1.6	1.7	5.3	16.2	0.01	0.10	0.21
M21-26 (1130 °C)	0.06	2.5	1.8	5.5	11.6	0.01	0.09	0.17
M22-18 (1110 °C)	0.05	5.4	1.6	4.9	12.1	0.01	0.07	0.16
M1-6 (1070 °C)	0.04	22.3	1.2	4.2	11.8	0.01	0.05	0.12
M5-13 (1050 °C)	0.04	36.1	1.4	5.5	15.1	0.01	0.04	0.08
Average	0.06	11.4	1.5	5.0	13.1	0.01	0.09	0.18

TABLE 8. Previously published olivine-melt *D*-values

Element	Reference D-value	Reference
V	0.014–0.019	Norman et al. 2005
Cr	1.32–4.52	Norman et al. 2005
Mn	1.17–1.69	Norman et al. 2005
Co	4.05–5.15	Norman et al. 2005
Ni	24.68–38	Norman et al. 2005
Ni	10.0–11.0	Papike et al. 1999
Y	0.01	Nikogosian and Sobolev 1997
Sm	0.11	Shimizu et al. 1982
Th	0.02	Dunn and Sen 1994

ment mechanisms, and microscopic melt-inclusions can produce anomalously high *D*-values in some samples (e.g., Shimizu et al. 1982). *D*-values can be also compromised if the analyzed minerals were not in equilibrium with the surrounding melt. As we have discussed in this paper, factors such as gravitational settling and convective flow can transport minerals to regions of the lake that have seen previous enrichments and/or depletions of specific trace elements.

D-values that are compromised by the disequilibrium between minerals and their surrounding melts are referred to as apparent *D*-values (Albarede and Bottinga 1972). Most workers view apparent *D*-values as meaningless; however, we propose that apparent *D*-values can be used to obtain information about the mechanisms that have acted on the basaltic system, especially when other physical and chemical data are unavailable. More specifically, we can use information about the way in which the apparent *D*-values (Table 7) deviate from the reference *D*-values (Table 8) to determine what mechanisms have affected the system.

It should be noted, however, that some apparent *D*-values can be influenced artificially by the analytical procedure itself. For instance, a depth-penetrating ion beam (i.e., SIMS beams) can incorporate small-scale melt inclusions that are not visible at the surface of the sample. The same SIMS beam may also incorporate the effects of mineral-melt interface reactions, which can occur within 50 µm of the mineral-melt interface. If either of these scenarios occur, the calculated *D*-values will be highly unusual for both compatible and incompatible elements but in a predictable way. For example, Kennedy et al. (1993) showed that melt inclusions will have low abundances of compatible elements and high abundances of incompatible elements compared to the host mineral. In fact, melt inclusions can be enriched in incompatible elements by a factor of up to 10^5 over the mineral (Kennedy et al. 1993). Therefore, the melt inclusions will cause the concentrations of compatible trace elements in the mineral to be anomalously low and the concentrations of incompatible elements to be anomalously high. These effects will in turn cause the apparent *D*-values to be too low for compatible elements and too high for incompatible elements relative to reference *D*-values.

The effects of mineral-melt interface kinetics can be also seen in the apparent *D*-values. More specifically, if the mineral analyses did not incorporate any melt inclusions, the influence of mineral-melt interface kinetics will cause the apparent *D*-values for compatible elements to be too high and the apparent *D*-values for incompatible elements to be too low compared to reference *D*-values. The effects on the apparent *D*-value will occur because glasses influenced by mineral-melt interface kinetics will have anomalously high concentrations of incompatible elements and anomalously low concentrations of compatible elements (Shimizu 1983).

Figures 10a and 10b show how the apparent olivine-melt *D*-values (D^{Ol}) from this study vary as a function of temperature and how they compare with reference D^{Ol}-values from other studies. Figures 10a and 10b show that the olivines from the high-temperature samples have D^{Ol}-values for compatible elements, such as Mn, Cr, Co and Ni, that appear to be too low and D^{Ol}-values for incompatible elements, such as V, Y, Sm, and Th, that appear to be too high relative to reference D^{Ol}-values. Noting the effects on apparent *D*-values described above, the anomalous D^{Ol}-values in Figures 10a and 10b can be explained by accidental analysis of melt inclusions, which have been identified in the MLL olivines (Fig. 11).

Identifying petrologic processes with apparent *D*-values

When the effects of mineral-melt interface kinetics and unintentional analysis of melt inclusions can be identified and subsequently accounted for, we can use the amount and style of deviation of apparent *D*-values away from reference *D*-values to obtain information about petrologic mechanisms. A comparison of our *D*-values with reference *D*-values shows that Mn, Co, Sm, and Y *D*-values from this study correlate very well with the reference *D*-values. The fact that our results for D_{Mn}, D_{Co}, D_{Sm}, and D_Y compare favorably with reference *D*-values indicates that the *D*-values for these elements are not affected easily by petrologic mechanisms and are therefore relatively robust.

Our calculated D_{Ni} is much lower than that reported by

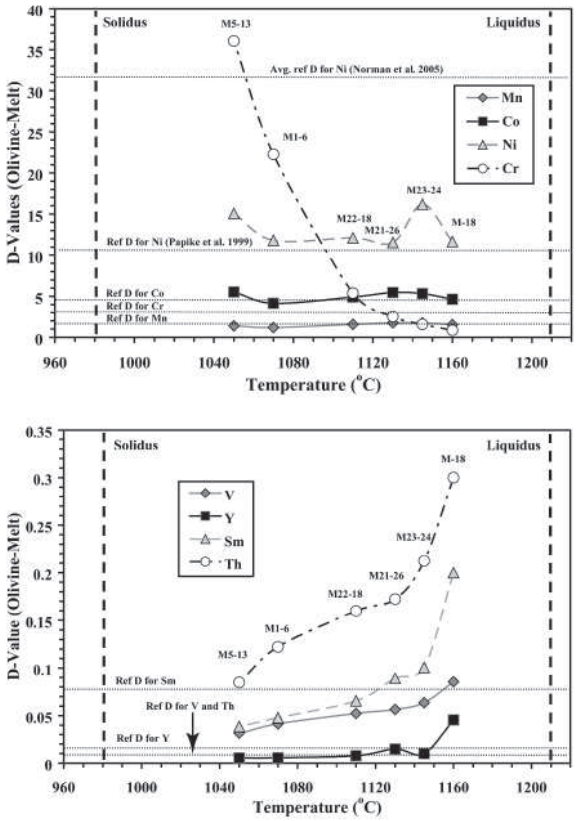

FIGURE 10. Olivine-melt *D*-values plotted as a function of temperature. The dotted horizontal lines represent reference *D*-values from previous studies (see Table 8 for actual values). (**a**) The *D*-values for Co and Mn agree well with the reference *D*-values. The deviations in the Cr *D*-values are caused by gravitational settling and/or convective flow (see text for discussion). (**b**) The high *D*-values in sample M-18 are the result of analyzing melt inclusions. The measured D_{Th} and D_{V}-values are higher than the reference *D*-values for Th and V.

FIGURE 11. Back-scattered electron image showing small-scale melt inclusions in an olivine grain from sample M23-24. The image is approximately 100 μm across.

Norman et al. (2005) but our average D_{Ni} fits in well with the ranges described by Papike et al. (1999) and Nabelek (1980). We assume that because Ni is highly compatible in the olivine structure (e.g., Papike et al. 1999), the apparent D_{Ni}-value for sample M-18 should be much higher than for the other samples and that the D_{Ni}-values for the other samples should decrease asymptotically (see examples in Hess 1989); however, because of the melt inclusions in the M-18 olivines, the apparent *D*-value for Ni in M-18 is anomalously low. The sudden upturn in the D_{Ni} trend line at 1050 °C can be explained by the fact that Ni is depleted in the melt by the crystallization of ilmenite, where $D_{Ni}^{Ilm} = 2.6$ (Mysen 1978).

Figures 10a and 10b show that our calculated *D*-values for V, Cr, and Th in the low-temperature samples are much different than published reference *D*-values. Given the above information, we propose that the Cr *D*-values in the low-temperature samples can be explained if Cr-rich olivines are co-located with Cr-poor glasses. In other words, because we know that Cr-rich olivines crystallized early, that Cr-poor glasses crystallized late, and that olivine grains in the MLL were transported to other parts of the lake via convective flow or gravitational settling, we can infer that the apparent *D*-values for Cr reflect the transport processes in the MLL. A similar effect is not as obvious in the *D*-values for other elements because Cr becomes extremely depleted in the residual melt with the crystallization of pyroxene, ilmenite, and chromite.

The *D*-values for V and Th, on the other hand, appear to be affected by factors other than gravitational settling or convective flow. Figure 10b shows that the calculated D_{Th} in all of the Makaopuhi samples is much higher than the reference value of 0.02 (i.e., Dunn and Sen 1994). In fact, the difference between the D_{Th}-values in the Makaopuhi samples and the D_{Th}-values predicted from experiments is more than an order of magnitude (compare Tables 7 and 8). The high D_{Th}-values reported in this study could reflect the fact that Th^{4+} is the slowest diffusing trace element in basaltic melts (Bindeman and Davis 1999). Because Th diffuses so slowly, it could be more prone to incorporation into a growing crystal. These results suggest that Th is partitioned more effectively into the olivine than has been suggested previously. A similar conclusion might be reached for V, which has apparent *D*-values that are consistently higher than the reference *D*-values (Fig. 10b). One recent study indicates that V in the MML is likely in the 4+ valence state (Karner et al. 2006) and therefore may also experience relatively slow diffusion in basaltic melts.

ACKNOWLEDGMENTS

This work was supported by a grant form the Institute of Geophysics and Planetary Physics (IGPP) (P.I.s C.K. Shearer and D.T. Vaniman) and by a student fellowship from the New Mexico Space Grant Consortium (J.J. Hagerty). The Division of Petrology and Volcanology, Department of Mineral Sciences, Smithsonian Institution, provided samples from the Makaopuhi Lava Lake. We thank Michael Garcia, Valerie Reynolds, and Ted Labotka for helpful reviews. We also thank James J. Papike for his invaluable contributions to the fields of mineralogy and planetary science.

REFERENCES CITED

Albarede, F. and Bottinga, Y. (1972) Kinetic disequilibrium in trace element partitioning between phenocryst and host lava. Geochimica et Cosmochimica Acta, 36, 141–156.

Bindeman, I.N. and Davis, A.M. (1999) Convection and redistribution of alkalis and trace elements during the mingling of basaltic and rhyolite melts. Journal of Petrology, 7, 91–101.

Chakraborty, S. (1995) Diffusion in silicate melts. In J.F. Stebbins, P.F. McMillan, and D.B. Dingwell, Eds., Structure, Dynamics and Properties of Silicate Melts, 32, p. 411–497. Reviews in Mineralogy, Mineralogical Society of America, Chantilly, Virginia.

Dunn, T. and Sen, C. (1994) Mineral/matrix partition-coefficients for ortho-pyroxene, plagioclase, and olivine in basaltic to andesitic systems—a combined analytical and experimental study. Geochimica et Cosmochimica Acta, 58, 717–733.

Grove, T.L. and Bence, A.E. (1979) Crystallization kinetics in a multiply saturated basalt magma: An experimental study of Luna 24 ferrobasalt. Proceedings of the 10th Lunar and Planetary Science Conference, p. 439–478.

Grove, T.L. and Raudsepp, M. (1978) Effects of kinetics on the crystallization of quartz normative basalt 15597: An experimental study. Proceedings of the 9th Lunar and Planetary Science Conference, p. 585–599.

Hart, S.R. and Davis, K.E. (1978) Nickel partitioning between olivine and silicate melt. Earth and Planetary Science Letters, 40, 203–219.

Hart, S.R. and Dunn, T. (1993) Experimental cpx/melt partitioning of 24 trace elements. Contributions to Mineralogy and Petrology, 113, 1–8.

Hess, P.C. (1989) Origins of Igneous Rocks, 336 p. Harvard University Press, Cambridge, Massachusetts.

Huebner, J.S. and Sato, M. (1970) The oxygen fugacity-temperature relationships of manganese oxide and nickel oxide buffers. American Mineralogist, 55, 934–952.

Karner, J.M., Sutton, S.R., Papike, J.J., Shearer, C.K., Jones, J.H., and Newville, M. (2006) Application of a new varadium valence oxybarometer to basaltic glasses from the Earth, Moon, and Mars. American Mineralogist, 91, 270–277.

Kennedy, A.K., Lofgren, G.E., and Wasserburg, G.J. (1993) An experimental study of trace element partitioning between olivine, orthopyroxene, and melt in chondrules: Equilibrium values and kinetic effects. Earth and Planetary Science Letters, 115, 177–195.

Kinzler, R.J., Grove, T.L., and Recca, S.I. (1990) An experimental study on the effect of temperature and melt composition of the partitioning of nickel between olivine and silicate melt. Geochimica et Cosmochimica Acta, 54, 1255–1265.

Kirkpatrick, R.J. (1977) Nucleation and growth of plagioclase, Makaopuhi and Alae lava lakes, Kilauea Volcano, Hawaii. Geological Society of America Bulletin, 88, 78–84.

McBirney, A.R. (1984) Igneous Petrology, 509 p. Freeman, Cooper, and Co., San Francisco, California.

Mysen, B. (1978) Experimental determination of nickel partition coefficients between liquid, pargasite, and garnet peridotite minerals and concentration limits of behavior according to Henry's Law at high pressure and temperature. American Journal of Science, 278, 217–243.

Nabelek, P.I. (1980). Nickel partitioning between olivine and liquid in natural basalts: Henry's Law behavior. Earth and Planetary Science Letters, 48, 293–302.

Nikogosian, I.K. and Sobolev, A.V. (1997). Ion microprobe analysis of melt inclusions in olivine: Experience in estimating the olivine-melt partition coefficients of trace elements. Geochemistry International, 35, 119–136.

Norman, M., Garcia, M.O., and Pietruszka, A.J. (2005) Trace-element distribution coefficients for pyroxenes, plagioclase, and olivine in evolved tholeiites from the 1955 eruption of Kilauea Volcano, Hawaii and petrogenesis of differentiated rift-zone lavas. American Mineralogist, 90, 888–899.

Papike, J.J. (1981) Silicate mineralogy of planetary basalts. In R.B. Merrill and R. Ridings, Eds., Basaltic Volcanism on the Terrestrial Planets, p. 340–363. Pergamon, New York.

——— (1996) Pyroxene as a recorder of cumulate formational processes in asteroids, Moon, Mars, Earth: Reading the record with the ion microprobe. American Mineralogist, 81, 525–544.

——— (1998) Comparative planetary mineralogy: Chemistry of melt-derived pyroxene, feldspar, and olivine. In J.J. Papike, Ed., Planetary Materials, 36, p. 7-01–7-10. Reviews in Mineralogy, Mineralogical Society of America, Chantilly, Virginia.

Papike, J.J., Ryder, G., and Shearer, C.K. (1998) Lunar samples. In J.J. Papike, Ed., Planetary Materials, 36, p. 5-01–5-05. Reviews in Mineralogy, Mineralogical Society of America, Chantilly, Virginia.

Papike, J.J., Fowler, G.W., Adcock, C.T., and Shearer, C.K. (1999) Systematics of Ni and Co in olivine from planetary melt systems: Lunar mare basalts. American Mineralogist, 84, 392–399.

Papike, J.J., Karner, J.M., and Shearer, C.K. (2003) Determination of planetary basalt parentage: A simple technique using the electron microprobe. American Mineralogist, 88, 469–472.

——— (2005) Comparative planetary mineralogy: Valence state partitioning of Cr, Fe, Ti, and V among crystallographic sites in olivine, pyroxene, and spinel from planetary basalts. American Mineralogist, 90, 277–290.

Ringwood, A.E. (1970) Petrogenesis of Apollo 11 basalts and implications for lunar origin. Journal of Geophysical Research, 75(32), 6154–6479.

Roeder, P.L. and Emslie, R.F. (1970) Olivine-liquid equilibrium. Contributions to Mineralogy and Petrology, 29, 275–289.

Sato, M. and Wright, T.L. (1966) Oxygen fugacities directly measured in magmatic gases. Science, 153, 1103–1105.

Shimizu, N. (1983) Interface kinetics and trace element distribution between pherocrysts and magma. In S.S. Augustithis, Ed., The Significance of Trace Elements in Solving Petrogentic problems and controversies, p. 175–194. Theophrastus Publications SA, Athens.

Shimizu, H., Sangen, K., and Masuda, A. (1982) Experimental study on rare-earth element partitioning in olivine and clinopyroxene formed at 10 and 20 kb for basaltic systems. Geochemical Journal, 16, 107–117.

Wright, T.L. and Okamura, R.T. (1977) Cooling and crystallization of tholeiitic basalt, 1965 Makaopuhi Lava Lake, Hawaii. Geological Survey Professional Paper, 1004, p. 78.

MANUSCRIPT RECEIVED SEPTEMBER 15, 2005
MANUSCRIPT ACCEPTED MAY 12, 2006
MANUSCRIPT HANDLED BY THEODORE LABOTKA